

# Optimisation of straight plate upstream deflector for the performance enhancement of vertical axis wind turbine at low, medium and high regimes of tip speed ratios

Wind Engineering  
2022, Vol. 46(5) 1487–1510  
© The Author(s) 2022



Article reuse guidelines:

sagepub.com/journals-permissions  
DOI: 10.1177/0309524X221084980  
journals.sagepub.com/home/wie



Taurista P. Syawitri<sup>1,2</sup> , Yufeng Yao<sup>1</sup>, Jun Yao<sup>1</sup> and Budi Chandra<sup>1</sup>

## Abstract

Location and geometry optimisations of Straight Plate Upstream Deflector (SPUD) for performance enhancement of a three-straightbladed Vertical Axis Wind Turbine (VAWT) are carried out at three regimes of tip speed ratios (TSRs). Results analysis reveals that SPUD location has significant effect on the power coefficient ( $C_p$ ) increment of VAWT. Placing two SPUDs both upward and downward in upstream of VAWT can achieve the highest  $C_p$  improvement at all regimes of TSRs. Overall, placing SPUD in upstream of VAWT can improve the  $C_p$  value at all regimes of TSRs, but the percentage of improvement can vary. The largest  $C_p$  improvement of 126.7% is achieved at low regime of TSRs, while at the medium and high regimes of TSRs,  $C_p$  improvements decrease to 52.7% and 52.5%, respectively. Increasing the width of SPUD can increase the average VAWT  $C_p$  improvement by 2.83% at all regimes of TSRs.

## Keywords

Vertical axis wind turbine, straight plate upstream deflector, stressblended eddy simulation, location and geometry optimisation, tip speed ratios

## Introduction

Compared to drag-driven Vertical Axis Wind Turbine (VAWT), lift-driven VAWT is much more promising to be utilised as a power generation device due to its higher efficiency. However, in order to compete with commercial Horizontal Axis Wind Turbine (HAWT), lift-driven VAWT still needs to improve its efficiency and self-starting ability. One method that has been proposed and implemented to improve these two characteristics is by using flow augmentation devices to improve the incoming wind conditions around the turbines. This method is proved to be very effective by increasing the mass flow rate through the augmented area, resulting in an increased VAWT efficiency close to or even beyond the Betz limit (i.e., 59.3%) (Wong et al., 2017).

Based on the augmented flow direction, flow augmentation devices can be divided into two types, namely single directional flow augmentation and omnidirectional flow augmentation. Single directional flow augmentation devices, such as guide vane row and tail vane (Takao et al., 2009), diffuser (Letizia and Zanforlin, 2016; Watanabe, et al., 2016), curve plate upstream deflector (Stout et al., 2017) and Straight Plate Upstream Deflector (SPUD) (Kim and Gharib, 2013, 2014; Jin et al., 2018; Wong et al., 2018a, 2018b), benefit from simple design and light weight. However, they only work in one single direction of augmented flow, while omnidirectional flow augmentation devices have the ability to augment the flow in any direction. Nevertheless, single directional flow

<sup>1</sup>Department of Engineering Design and Mathematics, University of The West of England, Bristol, UK

<sup>2</sup>Department of Mechanical Engineering, Universitas Muhammadiyah Surakarta, Surakarta, Central Java, Indonesia

## Corresponding author:

Yufeng Yao, Department of Engineering Design and Mathematics, University of The West of England, Bristol, BS16 1QY, UK.

Email: yufeng.yao@uwe.ac.uk

augmentation devices are more practical for VAWT applications, as omnidirectional flow augmentation devices such as omnidirectional guide vane (Chong et al., 2013; Wong et al., 2014) and omnidirectional stator (Nobile et al., 2014) are complicated in design and implementation. This study will focus on single directional flow augmentation and its application in VAWT.

Among single directional flow augmentation devices, SPUD has superior effectiveness, as it can improve the performance of VAWT while operating at all regimes of Tip Speed Ratios (TSRs) from low, medium to high (Wong et al., 2017). This is very important as VAWT tends to behave differently at different regimes of TSRs (Malael et al., 2014). Based on an evaluation of NACA 0021 aerofoil VAWT at low regime of TSRs (see, e.g., Castelli et al., 2011), it was found that during the operation, VAWT blades can experience higher angle of attacks ( $AoA$ s) (up to  $27.7^\circ$ ) beyond the stall angle of a static aerofoil (normally  $+15^\circ/-15^\circ$ ). This causes very small amount of positive or sometimes even negative torque production which leads to poor self-starting ability of VAWT at low wind speed or low TSRs operation (Malael et al., 2014). On the other hand, at medium regime of TSRs, VAWT blades will have small increment of  $AoA$ s beyond static stall angle compared to low regime of TSRs (up to  $10.3^\circ$  higher than the stall angle of a static aerofoil). As a result, the flow is mostly attached to the blade surfaces and the level of flow unsteadiness of VAWT can be decreased. At this regime of TSRs, optimum TSR operation can be obtained due to significant vortex shedding and wake flow appeared (Dixon, 2008). Lastly, at high regime of TSRs, VAWT can operate at  $AoA$  above static stall angle, but the margin would become smaller (up to  $5^\circ$  higher than the stall angle of a static aerofoil) compared to low and medium regimes of TSRs. Even though the turbine can operate at the static stall conditions and beyond, the power generation of VAWT will be largely reduced at high regime of TSRs. This is because at high regime of TSRs, the rotor of VAWT will act as a solid obstruction due to higher rotational speed, leading to stronger vibration, higher drag and larger tip losses (Bakırcı & Yılmaz, 2018; Ragheb & Ragheb, 2011).

More aforementioned, SPUD has the advantage of simpler design than most other single directional flow augmentation devices (e.g. a curved plate upstream deflectors that only give small performance increment, see Stout et al. (2017)) and has been widely applied in drag-driven VAWTs (Wong et al., 2017). The use of SPUD as a performance enhancement device for lift-driven VAWTs has also been investigated in several previous studies (Jin et al., 2018; Kim and Gharib, 2013, 2014; Wong et al., 2018a, 2018b). However, there are some limitations in those studies that need to be addressed. First, there is no investigation about the optimum location of the deflector in the upstream of lift-driven VAWT. For example, most of these studies (Jin et al., 2018; Kim and Gharib, 2013, 2014; Wong et al., 2018a, 2018b) choose one particular location at the upstream of VAWT (i.e., downward, upward or middle) without performing thorough parametric studies of the location and orientation effects, for example, the distance from the turbines in  $x$  and  $y$  directions. Second, most of previous studies only evaluated SPUD and performed geometry optimisation at a single regime of TSRs. It is known that flow around VAWT can behave quite differently depending on the TSRs regime of operation. One previous study did have evaluated geometry optimisations at wider regime of TSRs (Kim and Gharib, 2013). However, there was little explanation about the effect regime of TSRs on the geometry optimisations of SPUD with regard to the performance enhancement of VAWT. Third, there is little investigation on the use of SPUD for a single lift-driven VAWT with high solidity.

Therefore, the present study will address all these limitations identified in previous studies by including the location effect as well as performing geometry optimisation of SPUD at all regime of TSRs. Three regimes of TSRs at low, medium and high are considered with each regime of TSRs represented by one TSR value (e.g., low regime of TSRs = 1.44, medium regime of TSRs = 2.64 (optimum TSR), and high regime of TSRs = 3.3), due to similar behaviour of flow around VAWTs at the same regime of TSRs (Malael et al., 2014). A three-straight-bladed lift-driven VAWT configuration is adopted to accommodate higher solidity, and Computational Fluid Dynamics (CFD) is utilized to evaluate the effects of location and geometry of SPUD on the performance of lift-driven VAWT. In order to reduce the computational cost of running a full 3D simulation, a 2D plane cutting through the middle of 3D blades is considered and this approach has been widely used in design and optimisation process of devices that are utilized to improve the performance of VAWT (Acarer, 2020; Bianchini et al., 2019; Chen et al., 2015; Chong et al., 2013; Choudhry et al., 2016; Mohamed et al., 2020; Nobile et al., 2014; Sobhani et al., 2017; Stout et al., 2017; Yan et al., 2019a; 2019b, 2020). Moreover, it was concluded from the previous studies that 2D computational model of VAWT can give reasonable overall prediction on the performance and flow field around a rotor in the turbine mid-plane (Bianchini et al., 2017; Rezaeiha et al., 2018a). A hybrid Reynold-Averaged Navier Stokes-Large Eddy Simulation (RANS-LES) model applying Stress-Blended Eddy Simulation (SBES) together with Transition Shear-Stress Transport (TSST) turbulence model is applied for CFD simulations as this model can produce lower discrepancies of power coefficient ( $C_p$ ) prediction compared to other URANS turbulence

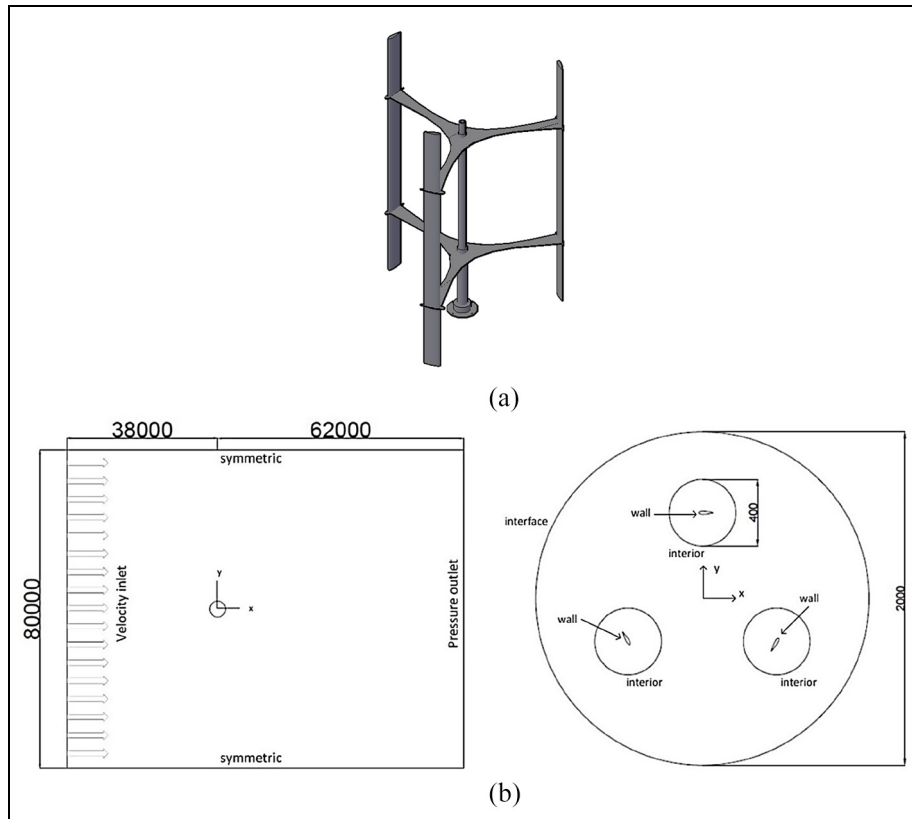


**Figure 1.** Bare VAWT model of Castelli et al. (2011), (a) 3D schematic of the turbine (experimental) and (b) 2D computational domain (not in scale; all measurements are in mm).

models (Syawitri et al., 2021) at all regimes of TSRs. All CFD simulations are carried out using ANSYS Fluent v19 (ANSYS, 2020).

## Geometry specification

### Bare VAWT

A bare VAWT adopted in this study is a three-straight-bladed lift-type VAWT with NACA 0021 aerofoil (see Figure 1) that has been studied experimentally and numerically by Castelli et al. (2011). This configuration has been widely used as a validation test case in several numerical studies (Ghazalla et al., 2019; Rezaeiha et al., 2019; Sobhani et al., 2017; Wang et al., 2018). Table 1 gives the main geometrical features and the operational parameters of both numerical and experimental models. In this study, all flow parameters are from Castelli et al. (2011). The bare VAWT is simulated over a wide regime of TSRs, particular at three TSRs regimes, namely low regime of TSRs (1.44–2.00), medium regime of TSRs (2.00–2.64 (optimum TSR)) and high regime of TSRs (2.64–3.3). The free stream velocity ( $U_\infty$ ) is set to be 9 m/s. The turbine rotational speed ( $\omega_t$  (rad/s)) is calculated based on equation 1.

$$TSR = \frac{\omega_t R}{U_\infty}, \quad (1)$$

where  $R$  (m) is the turbine radius.

### VAWT with straight plate upstream deflector

The effect of SPUD on VAWT performance improvement is investigated by placing straight plate deflector in upstream of a 2D plane cutting through the middle of a three-straight-bladed VAWT model. All turbine

**Table 1.** Main geometrical features and operational parameters of Castelli et al. (2011) model.

| Parameters                                 | Simulation               | Experiment          |
|--|--------------------------|---------------------|
| VAWT diameter ( $D_{rotor}$ (mm))          | 1030                     | 1030                |
| Blade height ( $H_{rotor}$ (mm))           | 1000 (for 2D simulation) | 1456.4              |
| VAWT swept area ( $A_s$ (m <sup>2</sup> )) | 1.03                     | 1.236               |
| Number of blade ( $N$ (-))                 | 3                        | 3                   |
| Blade profile                              | NACA 0021                | NACA 0021           |
| Chord length ( $c$ (mm))                   | 85.8                     | 85.8                |
| Trailing edge thickness (mm)               | 0.3792                   | 0.3792              |
| Spoke-blade connection                     | 0.25 of chord length     | 0.5 of chord length |
| Solidity ( $\sigma$ (-))                   | 0.5                      | 0.5                 |
| Aspect ratio                               | 1.4                      | 1.4                 |

**Table 2.** Geometry specification of a base SPUD.

| Parameter | Measurement      |           |
|-----------|------------------|-----------|
| $l_x$     | 1.02 $D_{rotor}$ | 1050 mm   |
| $l_y$     | 0.47 $D_{rotor}$ | 480.25 mm |
| $l_d$     | 6 mm             | 6 mm      |
| $w$       | 0.34 $D_{rotor}$ | 346.5 mm  |

geometries are kept the same as the bare VAWT model. A baseline SPUD geometry (see Table 2 and Figure 2, respectively) is adopted from a previous study of Kim and Gharib (2013) due to same regime of Reynolds number investigated.

For design optimisation, three parameters, namely location, width and inclination angle of the SPUD, are considered. First, the effect of four SPUD locations in upstream of VAWT (i.e., upward, middle, downward, and both upward and downward) on the average power coefficient over one turbine revolution ( $C_{p-ave}$ ) of VAWT is investigated. After identifying the SPUD location with the best performance, the effects of the width and inclination angle of SPUD on the  $C_{p-ave}$  production of VAWT are studied respectively. Noting that all of these investigations performed at all regimes of TSRs with  $TSR = 1.44$  represents low regime TSRs while medium and high regimes of TSRs are represented by  $TSR = 2.64$  and  $TSR = 3.3$ , respectively.

## CFD simulation

### Domain decomposition and grid generation

A C-type grid generation is adopted in this study. The simulation domain is divided into three sub-domains, namely the far-field, the rotating core and the control zone (see Figure 3). The far-field sub-domain is constructed by a C-shape together with a rectangular enclosure. The C-shape has  $25R$  in radius and the rectangular enclosure has  $30R$  in stream-wise distance from the centre of the turbine rotating axis to the exit plane as suggested by Zhu et al. (2018). SPUD is located in the far-field non-rotating sub-domain, surrounding the rotating core sub-domain. Hence, there is a slightly different approach to generate the grids in this domain between bare VAWT and VAWT with SPUD (see Figure 4). Structured grids are generated within the far-field sub-domain (see Figure 5(a)). The detailed grids around the deflector can be seen in Figure 5(b). Around the deflector, 50 grids are generated along the thickness of the deflector. Along the width of the deflector, 200 grids are created for the base SPUD. The number of grids increases with the increase of the width of the SPUD (see Table 3). The grids are distributed along both the thickness and width of the deflector by using finer grids to accommodate the near wall  $y^+$  criteria (e.g.,  $y^+ < 1$  for Transition SST turbulence model).

As mentioned above, the far-field sub-domain surrounds the rotating core sub-domain. This rotating core sub-domain is utilized to implement the revolution of the turbine, which is A circle shape domain with 2000 mm in diameter (about 1.94 times of the turbine diameter) is applied and it rotates in anti-clockwise direction around the

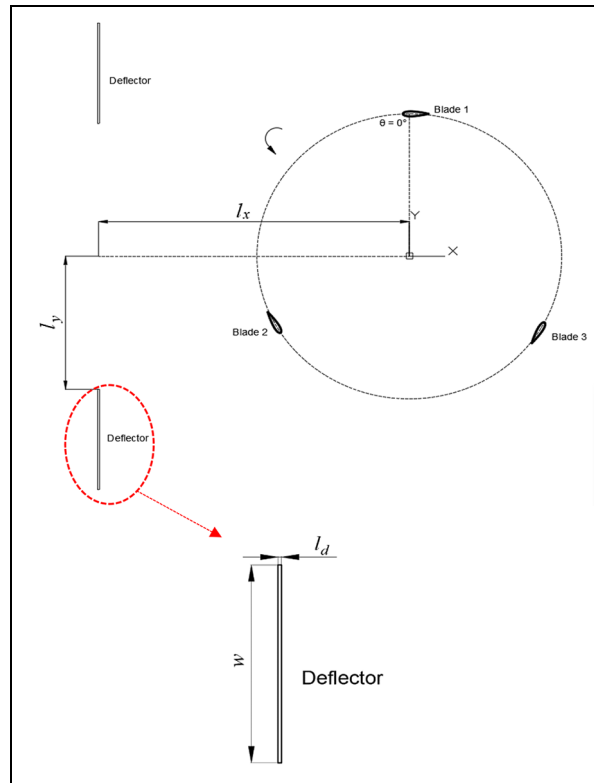


**Figure 2.** Detailed geometry of VAWT with SPUD, where  $l_x$  is a horizontal distance from the centre of the turbine (m),  $l_y$  is a vertical distance from the centre of the turbine (m),  $l_d$  is the thickness of the deflector (m) and  $w$  is the width of the deflector (m).

**Table 3.** Number of grids along the width of SPUD.

| Cases                          | Number of Grids along the Width of SPUD |
|--------------------------------|---|
| $w_0$ (base geometry)          | 200                                     |
| $w_1$ (25% of $w_0$ increment) | 250                                     |
| $w_2$ (50% of $w_0$ increment) | 300                                     |
| $w_3$ (75% of $w_0$ increment) | 350                                     |

rotating axis of the turbine at a given rotational speed. As mentioned in the previous studies (Balduzzi et al., 2016; Rezaeiha et al., 2018b), the size of rotating core needs to be at least around 1.5–2 times of turbine diameter to avoid unwanted disturbances produced by the sliding interface. Grids with quadrilateral dominant elements are implemented in this sub-domain (see Figure 6(a)). At the boundary intersection between the far-field and the rotating core sub-domains, a ‘fluid-fluid’ interface is set up to ensure the continuity of fluid flow cross these two sub-domains.

Inside the rotating core sub-domain, three control sub-domains with inserted blades are constructed for grid generation around the blades. These three control sub-domains are separated by  $120^\circ$  angular distance between the two adjacent blades. A C-shape with  $0.25R$  in radius and  $0.3R$  in length from the centre of the blade is used to construct each control sub-domain. Boundaries between three control sub-domains and the rotating core sub-domain are interpreted as “interior” to ensure the continuity of the fluid flow. Structured quadrilateral grids are generated in each control sub-domain, with fine grids in the near wall region (see Figure 6(b)) and coarse grids away from the wall. To satisfy the criteria of TSSST turbulence model, the non-dimensional wall distance  $y^+ < 1$  is adopted for generating the first layer height of the grid away from the wall of the blades.

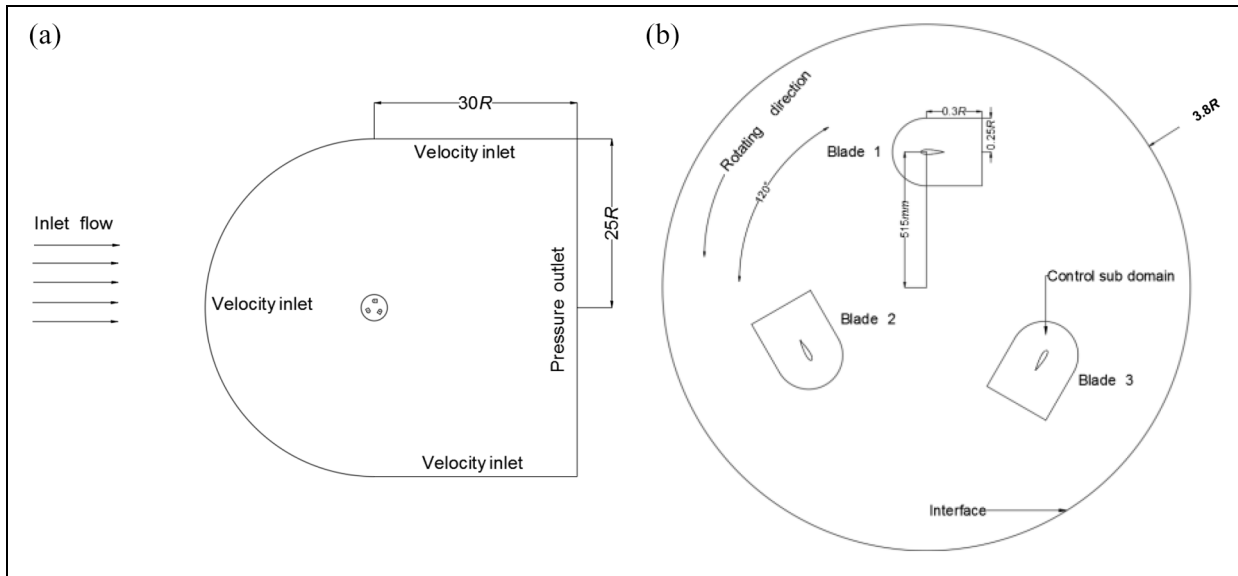


**Figure 3.** 2D computational domain and rotating core sub-domains. (a) Computational domain. (b) Rotating core sub-domain.

### Turbulence model

A hybrid RANS-LES turbulence model called Stress-Blended Eddy Simulation (SBES) is applied and this model is known for better resolving the Grid Induced Separation (GIS) issue occurred when the mesh is refined in the boundary layer region (Frank and Menter, 2017). This issue often appears in some hybrid RANS-LES turbulence models such as Detached Eddy Simulation (DES), Delayed-Detached Eddy Simulation (DDES) and Improved-Detached-Delayed Eddy Simulations (IDDES). The reason for GIS occurrence is mainly because there is improper balancing between RANS and LES turbulence contents due to the influence of LES grid limiter on the RANS model. In separating shear layers (SSL) region between RANS and LES zones, GIS can be triggered by the tendency of ‘slow’ transition from the RANS to the LES due to there is no clear differentiator between the two regions (Frank and Menter, 2017).

SBES turbulence model modifies the shielding function of the shielded DES (SDES) SST model by visualizing the shielding function and automatically switching to an existing algebraic LES model in the LES zone (Menter, 2018), thus to protect the RANS boundary layers and improve the ‘clearness’ of boundaries between the RANS and the LES zones. An explicit model is introduced to switch to an algebraic LES while maintaining the blending function the same as that of the shielding function SDES ( $f_{SDES}$ ) in the LES zone where  $f_{SDES} = 0$ . As a result, the turbulence stress tensor and the turbulence eddy viscosity equations are modified as

$$\tau_{i,j}^{SBES} = f_{SDES}\tau_{i,j}^{RANS} + (1 - f_{SDES})\tau_{i,j}^{LES}, \quad (2)$$

$$\nu_i^{SBES} = f_{SDES}\nu_i^{RANS} + (1 - f_{SDES})\nu_i^{LES}, \quad (3)$$

where  $\tau_{i,j}^{SBES}$ ,  $\tau_{i,j}^{RANS}$  and  $\tau_{i,j}^{LES}$  are turbulence stress tensors and  $\nu_i^{SBES}$ ,  $\nu_i^{RANS}$  and  $\nu_i^{LES}$  are turbulence eddy viscosities.

SBES model can be changed rapidly from the RANS to the LES shielding function in SSL region, due to its lower enforced turbulence stress level of LES model, which then can produce better, realistic, and consistent solutions. In addition, SBES model works well on a coarser grid for predicting a RANS-LES ‘switch’ compared to some hybrid RANS-LES turbulence models such as DES, DDES and IDDES so that the computational cost can be largely reduced.

### Computational settings

In order to solve the governing equations with hybrid RANS-LES model, a coupled numerical scheme for pressure-velocity coupling and a second-order scheme for temporal and spatial discretization are adopted in this study. A bounded central differencing scheme is implemented for momentum spatial discretization due to the

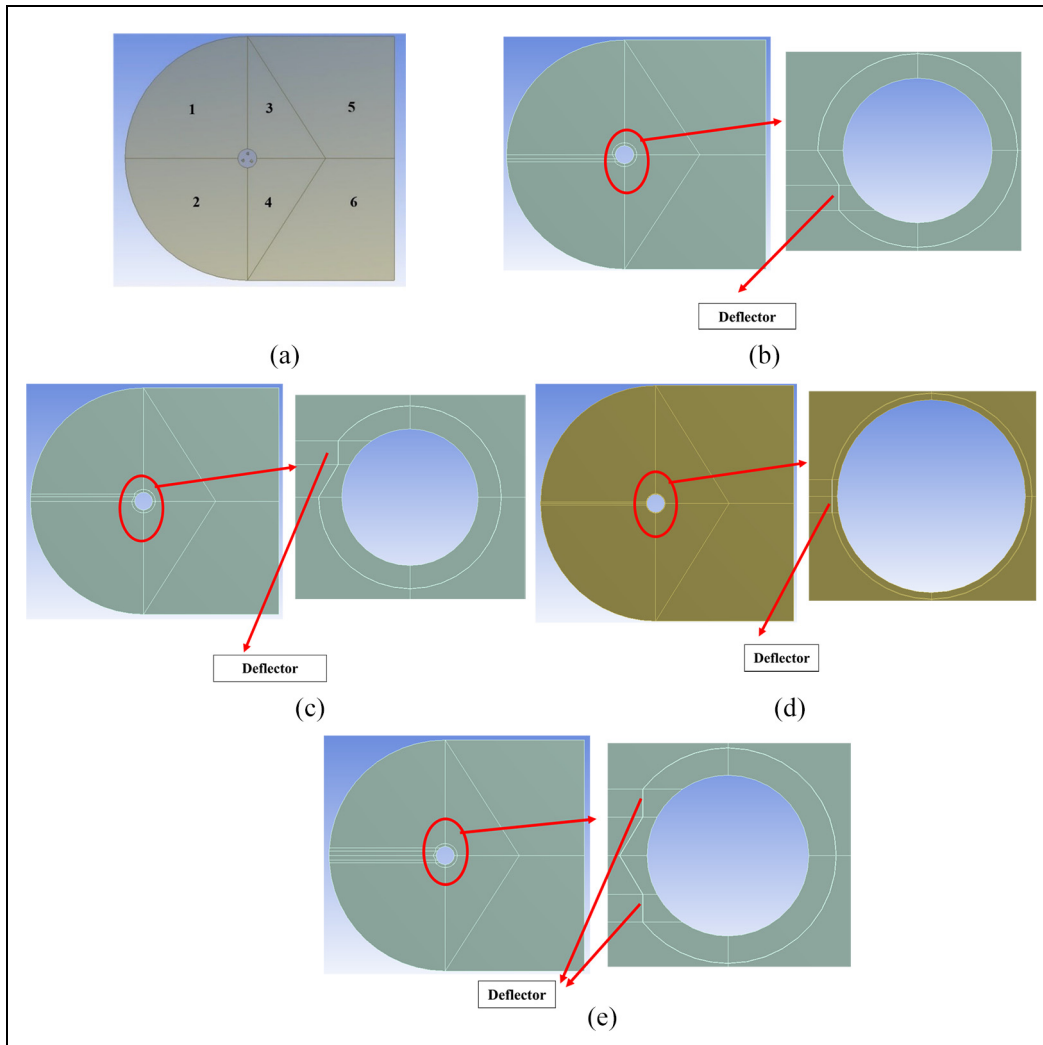


**Figure 4.** Comparison of the far-field sub-domain partition between base VAWT and VAWT with SPUD (four scenarios). (a) Base VAWT. (b) VAWT with a downward SPUD. (c) VAWT with an upward SPUD. (d) VAWT with a middle SPUD. (e) VAWT with both upward and downward SPUD.

requirement of hybrid RANS-LES turbulence model. All residual convergence criteria for the inner loop are set to be equal to or less than  $10^{-6}$ . A total of 40 sub-iterations per time step is applied as suggested by Balduzzi et al. (2016) and this setting can reduce the turbulence kinetic energy residuals by an order of  $10^{-4}$ .

In this study, the time step is set to be equal to the lapse time of a rotor making a  $1^\circ$  rotation. It was found that this time step is sufficient for a stable VAWT simulation (Syawitri et al., 2020, 2021). Final results of statistically converged data are retrieved from the 35<sup>th</sup> revolution, based on previous studies (Syawitri et al., 2020, 2021) which have revealed that simulation using SBES model with Transition SST generally requires 34 revolutions before the difference of moment coefficient ( $C_m$ ) between two neighbouring revolutions becomes less than 0.1%.

### Model validation

The grid independence and model validation studies of VAWT CFD simulation have already been documented in the work published by present authors (Syawitri et al., 2020, 2021). In summary, three grid resolutions from coarse, medium, to finer meshes, each having 87, 174 and 348 cells around the blade, were considered for grid independence studies (Syawitri et al., 2020). Figure 7 gives instantaneous moment coefficient ( $C_{mi}$ ) variations along azimuthal position, illustrating a small difference between the medium and the fine grids whilst the coarse grid could

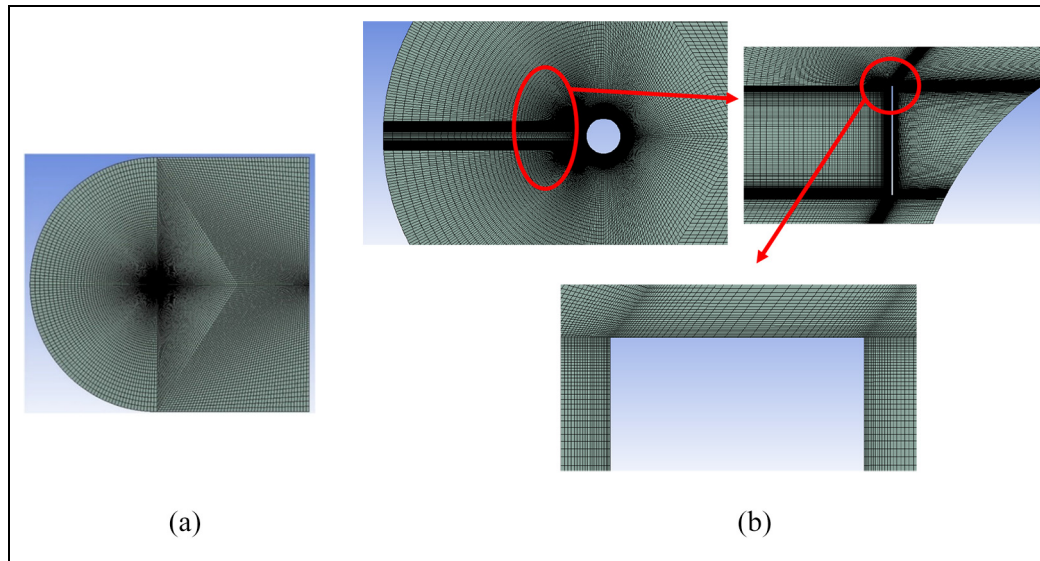


**Figure 5.** Detailed grids within the far-field sub-domain. (a) Detailed grids in the far-field sub-domain of a bare VAWT. (b) Detailed grids in the near wall region of SPUD.

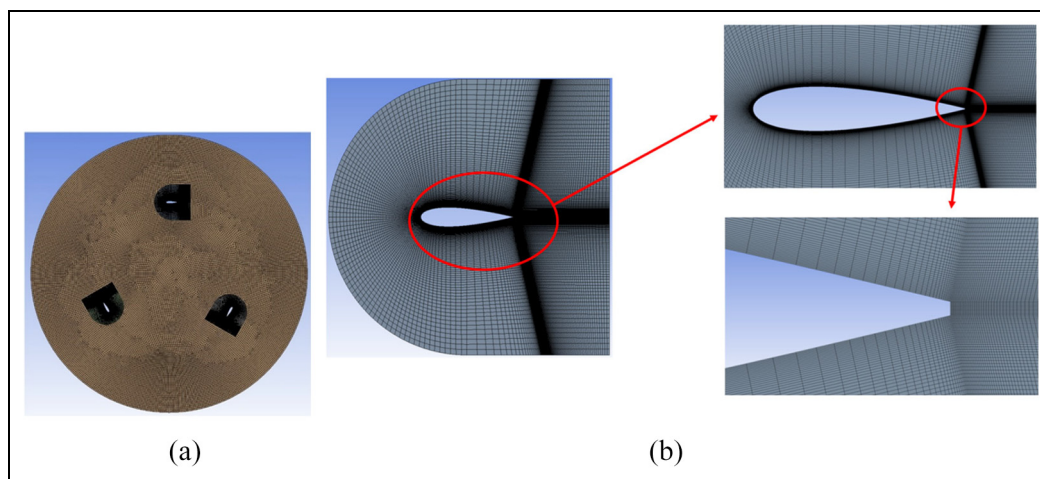


**Figure 6.** Detailed grids within (a) rotating core and (b) control sub-domains.

not produce satisfying instantaneous moment coefficients (Syawitri et al., 2020). These studies (Syawitri et al., 2020, 2021) have also found that better  $C_{p-ave}$  predictions can be produced even with the same turbulence model used by Castelli et al. (2011) and this is likely due to the improved grid quality, smaller time step and higher order of residual convergence criterion and increased number of internal iterations (Syawitri et al., 2021).

Moreover, these previous studies have found that SBES with TSST turbulence model has the ability to significantly reduce the discrepancy of power coefficient between CFD prediction and experiment results at all TSRs operations, compared to URANS turbulence models (Syawitri et al., 2020, 2021). In particular, SBES with TSST model is superior compared to URANS realizable  $k-\varepsilon$  turbulence model with enhanced wall treatment (RKE) that was used in the study of Castelli et al. (2011) at low regime of TSRs only. The  $C_{p-ave}$  prediction shows that RKE turbulence model produces nearly 450% of discrepancy compared to experiment data while SBES with TSST can reduce this discrepancy to less than 60% at low regime of TSRs. The ability of SBES with TSST turbulence models to improve the  $C_{p-ave}$  prediction is also found better than RKE turbulence models at the medium and high regimes of TSRs. While RKE generates about 16% of discrepancy compared to experiment data, SBES with TSST



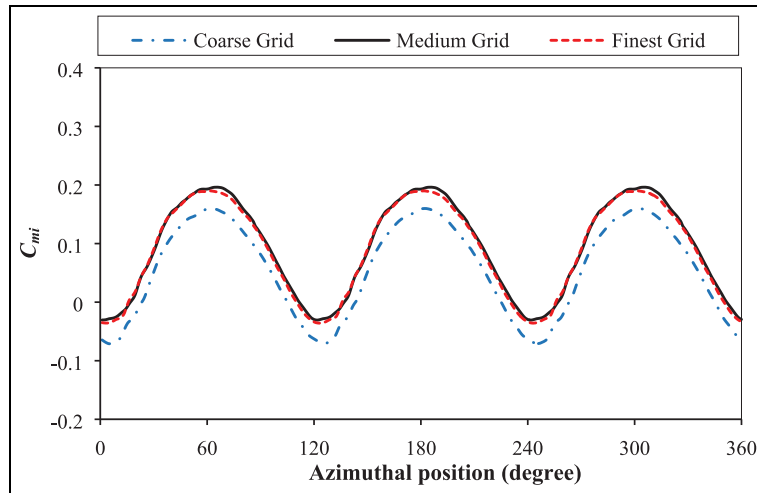


**Figure 7.** Comparison of instantaneous moment coefficients of VAWT with different grid resolutions for C-grid (Syawitri et al., 2020).

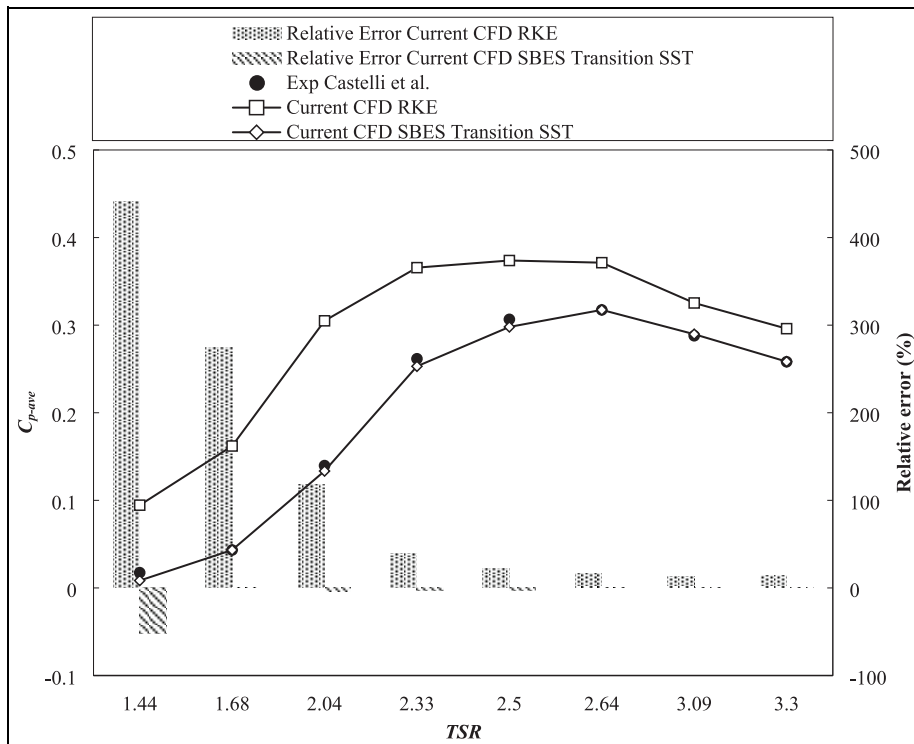


**Figure 8.** Comparison of average power coefficients between the experiments of Castelli et al. (2011) and current CFD simulation as well as relative errors in percentage (Syawitri et al., 2020).

produces very small discrepancy of around 1% compared to experiment data (see Figure 8). Furthermore, SBES model was found to have the ability to predict accurate dynamic stall behaviour, compared to RANS turbulence models as implicated by vortex shedding away from near blade wall. In addition, weak trailing edge rolling up at high regimes of TSRs can be predicted by SBES with TSST turbulence model while URANS turbulence models only capture weak vortex shedding around the trailing edge (Syawitri et al., 2021).

**Table 4.** Predicted  $C_{p-ave}$  values from four SPUD locations compared to bare VAWT (**bold** fonts indicate the optimum cases).

| Position  | $C_{p-ave}$     |                 |                 |
|-----------|-----------------|-----------------|-----------------|
|           | TSR = 1.44      | TSR = 2.64      | TSR = 3.3       |
| Bare VAWT | 0.008502        | 0.317431        | 0.261656        |
| Downward  | 0.008950        | 0.320839        | 0.271715        |
| Middle    | 0.015753        | 0.364896        | 0.297980        |
| Upward    | 0.018643        | 0.402920        | 0.386776        |
| Both      | <b>0.019274</b> | <b>0.484587</b> | <b>0.399071</b> |

It is worth noting that the primary purpose of this 2D simulation study is to perform geometry optimisation of SPUD as a practical solution for performance enhancement of VAWT at all regimes of TSRs, while still having reasonable accuracy. As mentioned above, this study evaluates a 2D plane cutting through the middle of 3D blade configuration. Previous study showed that a small discrepancy in power and moment coefficients predictions between 3D experiment and 2D CFD simulation, while 2D simulation represents the mid-plane of a turbine blade of high aspect ratio; where some 3D effects such as tip effects are small (Rezaeiha et al., 2017). While a full 3D simulation of experiment device is preferable to capture 3D flow features, a previous study using a hybrid LES-RANS model (DDES) showed that 2D simulation could produce relatively similar results as 3D simulation of turbulent flow separation on the blade (Lanzafame et al., 2020) as long as the spatial and temporal discretisation are fine enough to resolve the high vorticity gradients near the blades. Therefore, this study has focussed on 2D simulations to evaluate and optimise the key SPUD location and geometry parameters changes and its impact on turbine performance. Noting that, it takes about 100 hour CPU time on average to simulate one case using a high-spec workstation with 2 CPUs @ 2.2 GHz, and 128 GB RAM.

## Results and Discussion

### Effects of the location of upstream deflector

The effect of the SPUD location on the performance of VAWT is investigated considering four deflector locations in upstream of VAWT, that is, upward, downward, middle and both upward and downward (as shown in Figure 9). Table 4 gives the results showing that all four SPUD locations can improve the  $C_{p-ave}$  value compared to the bare VAWT at all regimes of TSRs. Moreover, the best  $C_{p-ave}$  improvement can be achieved by SPUD located at both upward and downward of the upstream of VAWT at all regimes of TSRs, followed by upward and middle configurations, respectively. The least  $C_{p-ave}$  improvement is generated by SPUD located at downward for all regimes of TSRs.

Noting that, due to the similar performance of each SPUD at all regimes of TSRs (see elaborations on Table 4 results), only TSR = 2.64 results are further discussed here (i.e., TSR with optimum  $C_{p-ave}$  value). Figure 10 depicts the effect of SPUD location on the instantaneous moment coefficient ( $C_{mi}$ ) distribution of VAWT at TSR = 2.64. It can be observed that only upward and both upward and downward configurations that can remove the negative moment production of VAWT. Meanwhile, for the middle and downward configurations, the negative moment is still generated by VAWT. It is also noticeable that all four configurations decrease the optimum moment coefficient of VAWT. Nevertheless, it is found that all four SPUD locations investigated can improve the averaged value of moment coefficient ( $C_{m-ave}$ ) compared to bare VAWT. For example, VAWT with SPUD of both upward and downward configuration can improve  $C_{m-ave}$  of bare VAWT from 0.12024 to 0.18356 at TSRs = 2.64. Hence, VAWT with four SPUD locations studied can produce better  $C_{p-ave}$  values (up to max 52.7% at TSR = 2.64 in case of applying both upward and downward SPUD) to bare VAWT.

Further investigation of flow streamlines indicates that placing SPUD at both upward and downward of the upstream of VAWT has the ability to induce larger vortex in upstream of VAWT compared to other three configurations (i.e. upward, middle and downward arrangements) (see Figure 11). This leads to stronger wake flow, resulting in greater augmented wind speed and direction change in downstream of the deflector where VAWT is located. In both upward and downward configuration, the VAWT blades can avoid the near wake region of the deflector while they are rotating. Meanwhile, for other three configurations of upward, middle and downward configurations, at least one blade will enter the near wake region of the deflector while the blades are rotating. Therefore, both upward and downward configuration can generate better power coefficient than other three

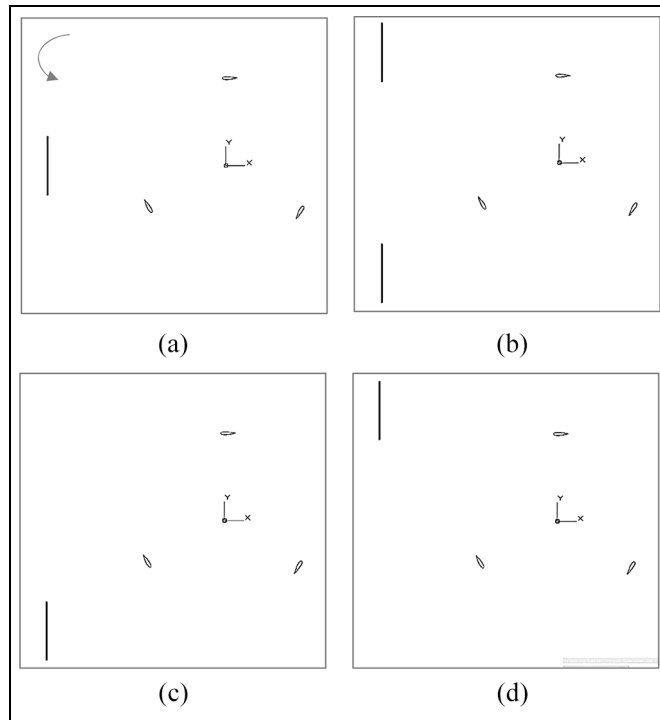


**Figure 9.** Sketches of four SPUD locations (the deflector geometry is not in scale), (a) middle, (b) both upward and downward, (c) downward and (d) upward.

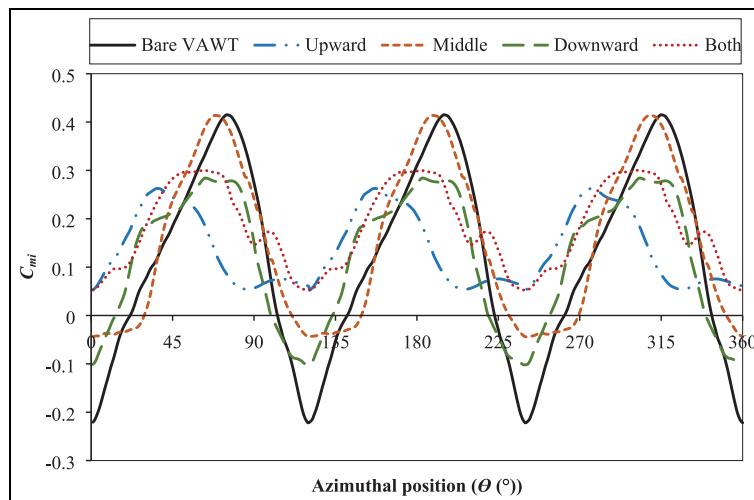


**Figure 10.** Comparison of instantaneous total moment coefficients (three blades) distributions of bare VAWT and VAWT with SPUD at four different locations (TSR = 2.64).

configurations. This finding is in good agreement with previous study (Kim and Gharib, 2013) by placing VAWT outside the near wake region of the deflector enabling to increase the power enhancement of VAWT. Moreover, both upward and downward configuration is observed better in directing the incoming wind towards the VAWT compared to upward, middle and downward configurations (see Figure 11). Since both upward and downward configuration introduce a nozzle-like effect in upstream of VAWTs, there is a decrease in the flow areas in the upstream of VAWT due to the gap between two deflectors. Apart from it can accelerate local wind speed, this effect can also help to re-direct the wind towards the turbines.

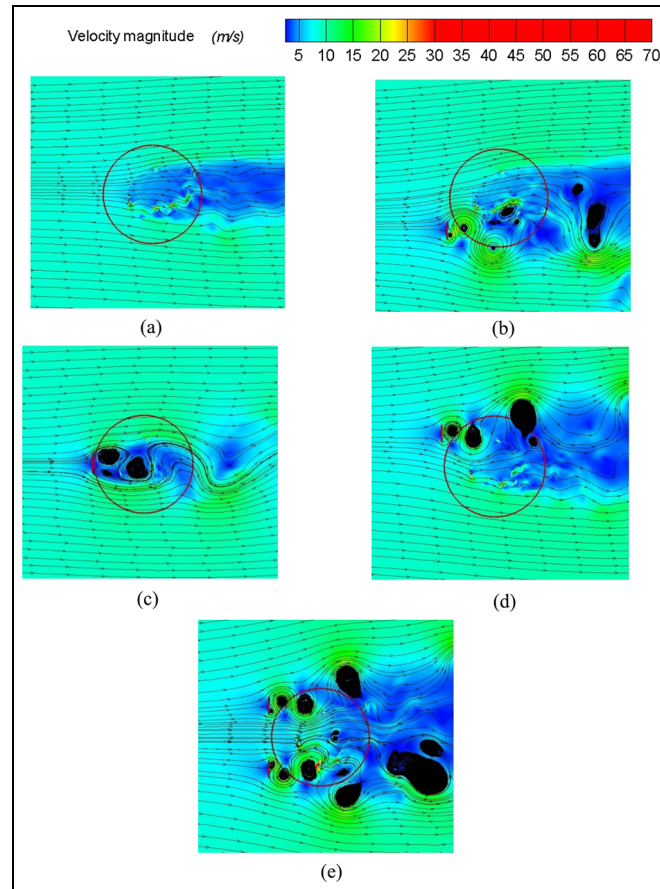


**Figure 11.** Comparison of streamline distributions coloured by velocity magnitude (m/s) of the flow around (a) bare VAWT and VAWT with SPUD at (b) downward, (c) middle, (d) upward and (e) both upward and downward (TSR = 2.64,  $\theta = 360^\circ$ ). The circles in dark solid lines represent the rotating core sub-domain.

Moreover, based on Figures 11(b) and 11(c), both downward and middle configurations can induce strong vortex flow motions between the blades of VAWT, compared to the upward and both upward and downward configurations which do not generate this kind of vortex flow motions (see Figures 11(d) and 11(e), respectively). This is possibly the main reasons behind the less  $C_{p-ave}$  improvement from these two former configurations. Furthermore, based on mean pressure contours of Blade 2 depicted in Figures 12(b) and 12(c), the downward and middle configurations can only reduce the pressure on the pressure side but still maintain similar pressure around the leading edge of the blade compared to bare VAWT (see Figure 12(a)). Noting that, the blade 2 is chosen because it is located at a position most exposed by the augmented wind, therefore it has made the largest contribution to the pressure changes at the investigated azimuthal position (i.e.,  $\theta = 360^\circ$ ) as shown in Figure 13. In addition, the upward and both upward and downward configurations can also reduce the pressure around the leading edge of the blade significantly (see Figures 12(d) and 12(e), respectively). Hence, the pressure gradient will be increased accordingly, resulting in higher moment generation and better power production.

It is also found that the existence of SPUD in upstream of VAWT can improve the  $C_{p-ave}$  of VAWT at all regimes of TSRs. However, the level of  $C_{p-ave}$  improvement varies at each regime of TSRs. SPUD can generate better improvement at low regimes of TSRs compared to medium and high regimes of TSRs. For example, in case of both upward and downward configurations, SPUD can improve the  $C_{p-ave}$  value by around 126.7% at low regime of TSRs compared to bare VAWT, while at medium and high regimes of TSRs,  $C_{p-ave}$  value can only be enhanced by approximately 52.7% and 52.5%, respectively. Note that the level of  $C_{p-ave}$  improvement reduces significantly until TSR = 2.5 (see Table 5). After that, the  $C_{p-ave}$  improvement continues to decrease but only slightly less than 0.1%. Similar behaviour is also noticed for other three configurations studied. It is believed that this behaviour is mainly caused by the augmented wind speed that is more beneficial at low regime of TSRs compared

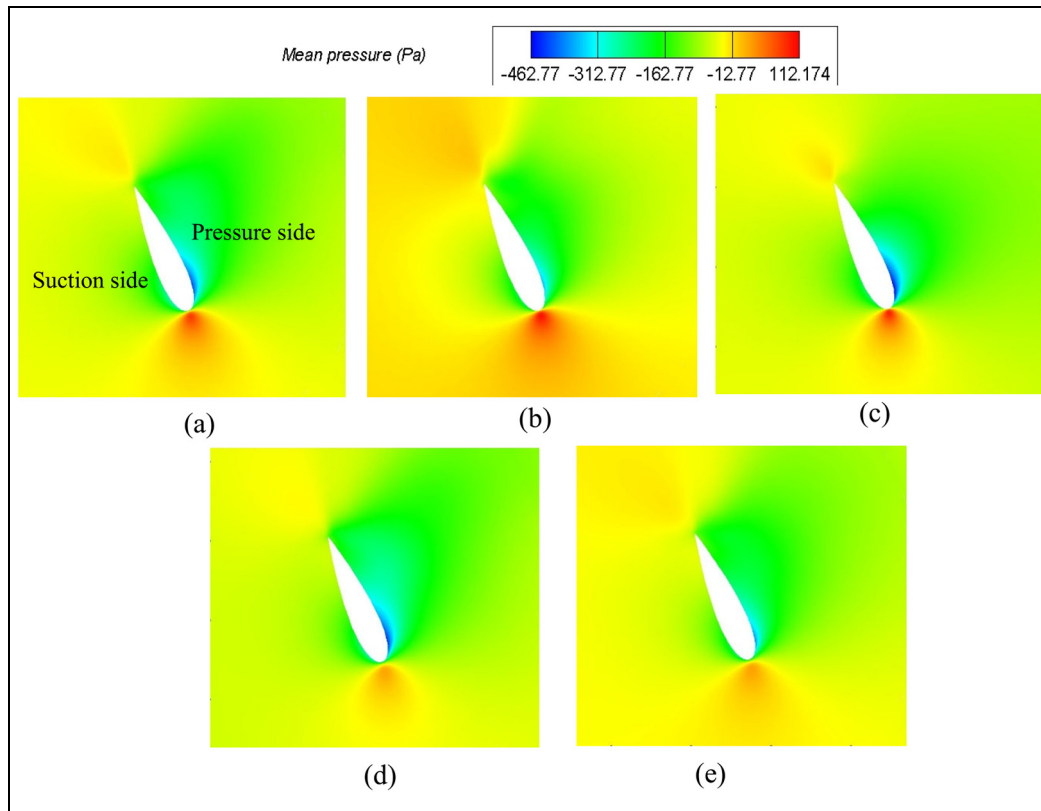


**Figure 12.** Comparison of mean pressure (Pa) contours of Blade 2 of (a) bare VAWT and VAWT with SPUD at (b) downward, (c) middle, (d) upward and (e) both upward and downward (TSR = 2.64,  $\theta = 360^\circ$ ).

to medium and high regimes of TSRs. At low regime of TSRs, the turbine rotation speed is quite slow so that the turbine usually needs external power to start the rotation until the turbine can self-rotate to produce positive power production. The higher incoming wind speed induced by the SPUD will help the turbine rotates faster after the rotation starting point. It is clear that SPUD can sometimes help the turbines to self-rotate without any external power and improve the power production significantly afterwards. However, at medium and high regimes of TSRs, the turbine rotation speed is already high. The higher rotation speed caused by higher incoming wind speed can induce the blockage effect to the flow with the addition of higher structure vibration and drag and tip losses in case of 3D VAWT configurations. Therefore, at these regimes of TSRs, the benefit of SPUD would be less significant in the start-up stage of VAWT.

Figure 14 illustrates the  $C_{mi}$  distributions of a bare VAWT compared with a VAWT of SPUD (i.e. both upward and downward configuration) at different regimes of TSRs. The  $C_{mi}$  distributions at TSR = 1.44 indicate that adding a deflector in upstream of VAWT can reduce the negative moment production of VAWT while still maintaining the optimum value of the positive moment. However, at TSR = 2.64, even though SPUD can remove the negative moment production of VAWT, it also reduces the optimum moment value of VAWT. This means that at low regime of TSRs, the SPUD can help VAWT to produce higher moment increment compared to medium and high regimes of TSRs. Nevertheless, the SPUD at TSR = 1.44 can reduce the fluctuations of the moment production. While at TSR = 2.64, it increases the fluctuations of the moment production. This is possibly caused by the higher drag as the turbine rotation speed increases at higher regimes of TSRs. Therefore, upstream deflector (for all location configurations) is proved as a device to improve the power generation of VAWT at all regime of TSRs, regardless of its lower effectiveness at medium and high regimes of TSRs.

The ability of SPUD to reduce negative moment production and ease its fluctuations at low regime of TSRs can help VAWT to improve its self-starting ability, which is very important at this regime of TSRs. In fact, SPUD can also reduce the cut-in wind speed at the lowest TSR operation (TSR = 1.44). The evaluation of  $C_{p-ave}$  value of bare VAWT at TSR = 1.44 shows that the bare VAWT starts to generate negative averaged moment (thus it

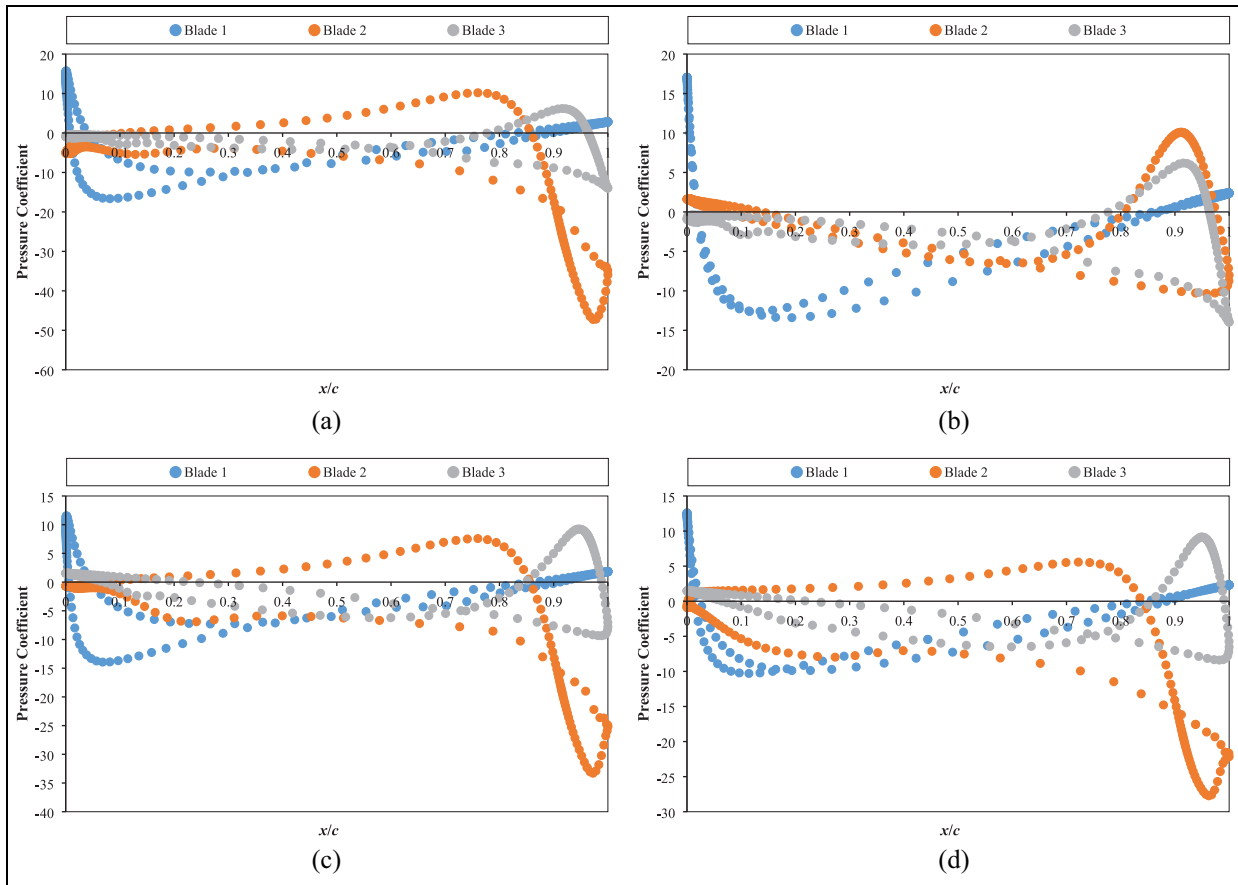


**Figure 13.** Comparison of pressure coefficient distributions of VAWT with SPUD at (a) downward, (b) middle, (c) upward and (d) both upward and downward (TSR = 2.64,  $\theta = 360^\circ$ ).

**Table 5.** Comparison of  $C_{p-ave}$  improvement due to SPUD of both upward and downward configuration at different TSRs.

| TSR  | $C_{p-ave}$ |                |                 |
|------|-------------|----------------|-----------------|
|      | Bare VAWT   | VAWT with SPUD | Improvement (%) |
| 1.44 | 0.00850     | 0.01927        | 126.7           |
| 1.68 | 0.04332     | 0.07742        | 78.7            |
| 2.04 | 0.13346     | 0.23207        | 73.9            |
| 2.33 | 0.25302     | 0.41826        | 65.3            |
| 2.5  | 0.29798     | 0.45696        | 53.4            |
| 2.64 | 0.31743     | 0.48459        | 52.7            |
| 3.09 | 0.28968     | 0.44194        | 52.6            |
| 3.3  | 0.26166     | 0.39907        | 52.5            |

cannot produce power) at incoming wind speed of  $U_\infty = 4.3$  m/s. The present SPUD in upstream of VAWT can reduce this cut-in wind speed to  $U_\infty = 3.5$  m/s. This means that VAWT with SPUD can start to produce power at lower incoming wind speed, resulting in better self-starting ability of VAWT.

### Effects of the width of upstream deflector

After obtaining the optimum location to place the deflector in upstream of VAWT, investigations are continued on the effect of the width of upstream deflector on the performance of VAWT. The width of upstream deflector

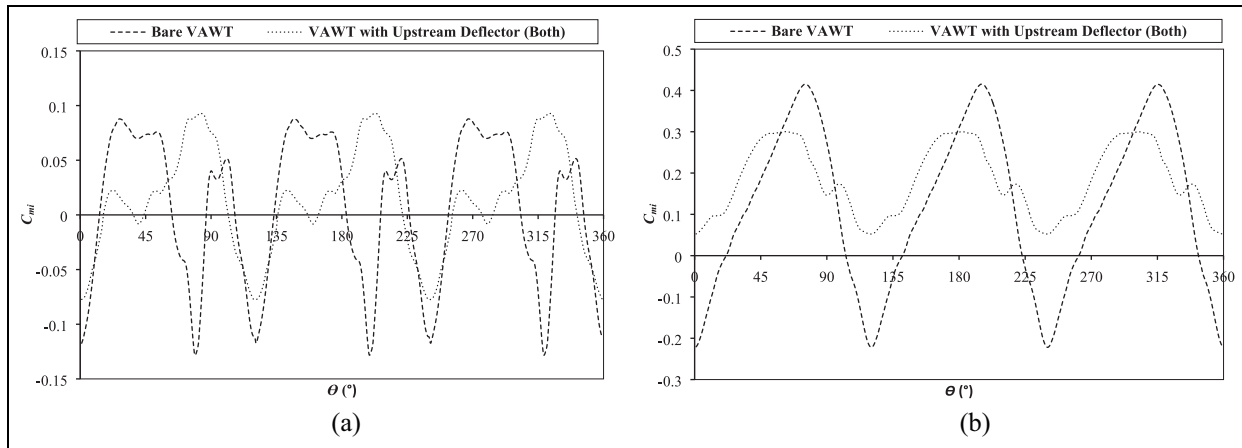


**Figure 14.** Comparison of  $C_{mi}$  distributions between bare VAWT and VAWT with SPUD (both upward and downward configuration) at (a) TSR = 1.44 and (b) TSR = 2.64.

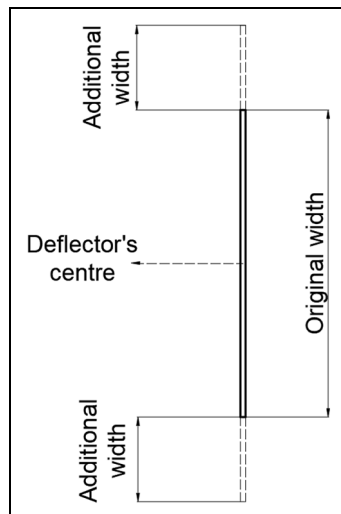


**Figure 15.** SPUD with width addition.

increases from the base SPUD of both upward and downward configuration by increasing the width of deflector on both ends (i.e., upward and downward) simultaneously. Note that this width addition is extended from the top and bottom ends of the deflector so that the centre of the deflector remains unchanged (see Figure 15). As a result, the gap between the two deflectors in both upward and downward configuration decreases as the width of the deflectors increases.

Simulations are carried out for three width variations ( $w_1$ ,  $w_2$  and  $w_3$ ) and results are compared with the base width ( $w_0$ ) as shown in Table 3. As the width is extended from the centre of the deflector, additional width at each end of deflector is a half of the width increment (e.g., in case of  $w_1$ , the width increment is 25% of  $w_0$ , this means that the width is extended 12.5% of  $w_0$  at each side of deflector). Figure 16 illustrates the effect of width variations on the  $C_{p-ave}$  production of VAWT with SPUD. The results have shown that all width variations investigated can produce better  $C_{p-ave}$  compared to bare VAWT at all regimes of TSRs. At each regime of TSRs, the increment of deflector width can improve the  $C_{p-ave}$  of VAWT until reaching an optimum value of  $C_{p-ave}$  improvement at  $w = 50\%$  of  $w_0$ . Compared to original width, SPUD with  $w = 50\%$  of  $w_0$  can further the improvement of  $C_{p-ave}$  by 5.5%, 1.2% and 1.7% at low, medium and high regimes of TSRs, respectively. Further increment of the deflector width will reduce the  $C_{p-ave}$  value of VAWT by 3.63%, 1.26% and 0.65% at low, medium and high regimes of TSRs, respectively, compared to optimum width (see Figure 17). The higher power generation of VAWT by the

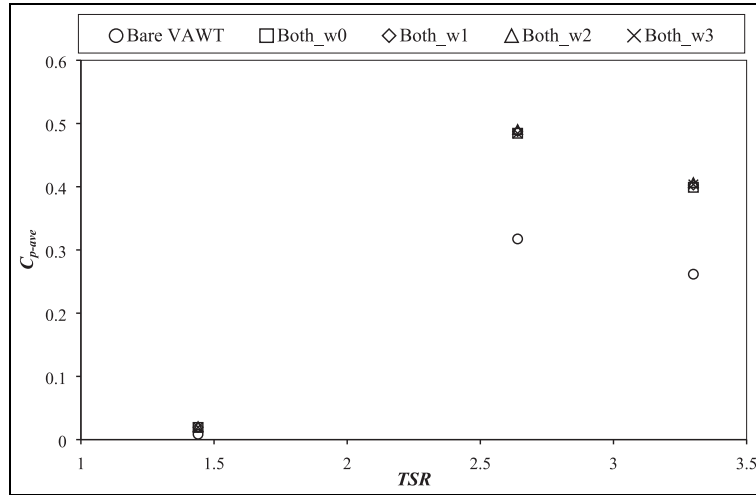


**Figure 16.** Comparison of  $C_{p-ave}$  between bare VAWT and VAWT with SPUD of both upward and downward configuration with four different width variations at different regimes of TSRs.

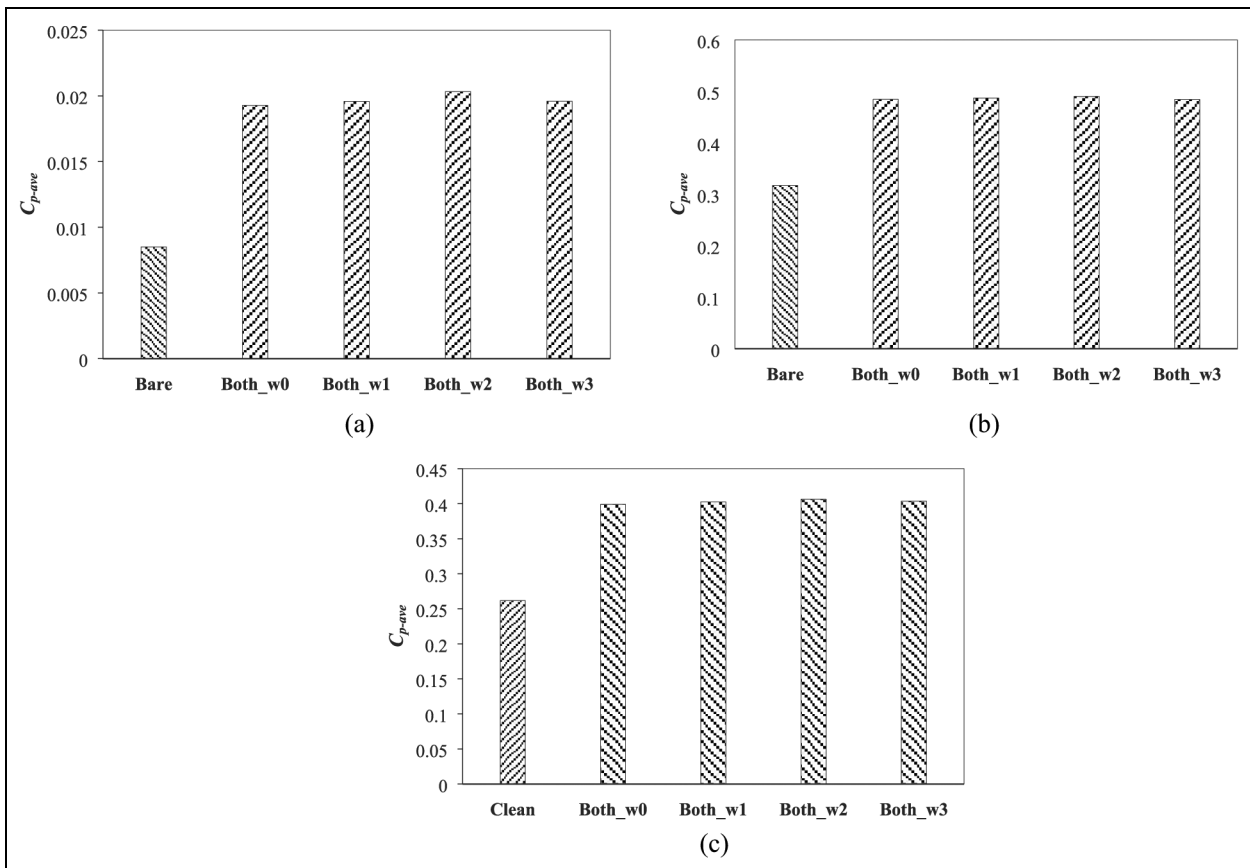


**Figure 17.** Comparison of  $C_{p-ave}$  between bare VAWT and VAWT with SPUD of both upward and downward configuration with four different width variations at (a) TSR = 1.44, (b) TSR = 2.64 and (c) TSR = 3.3.

increment of deflector width could be due to the decreased gap between two deflectors as the width of deflector increases. Based on the law of mass conservation, the flow velocity will rise at the outlet if the outlet area decreases. Hence, the local incoming wind speed increases as the gap between two deflectors decreases (as



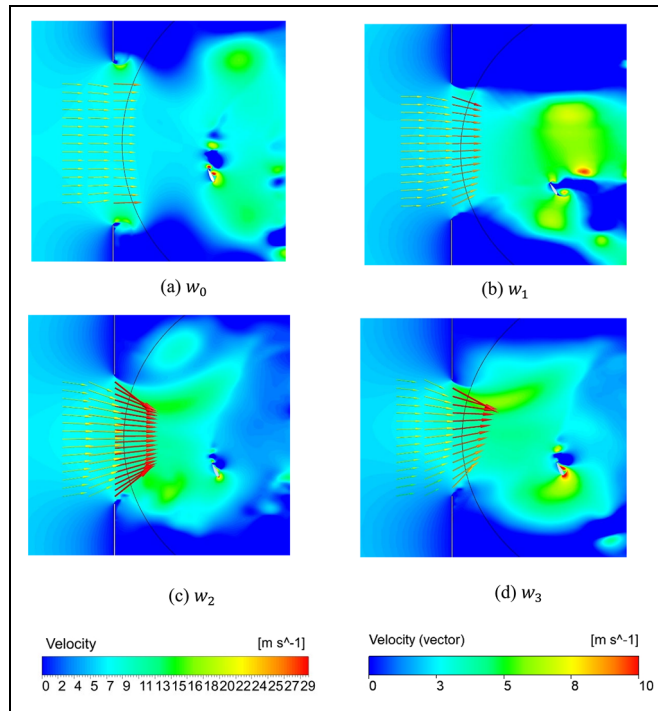


**Figure 18.** Comparison of velocity vectors, superimposed by contours coloured by velocity of VAWT with SPUD in different widths ( $TSR = 2.64$ ,  $\theta = 360^\circ$ ).

shown in Figure 18). The velocity vector and mean velocity contours have shown that there is velocity increment inside the gap between two deflectors as this gap decreases.

However, once  $w$  is greater than 50% of  $w_0$ , this incoming velocity improvement starts to reduce. This probably due to the fact that the increment of deflector width can lead to develop larger wake behind the deflector (see Figure 19). This larger wake can affect the ability of deflector to improve the VAWT performance as the velocity of the flow is not fully recovered before entering the turbine areas. Hence, this adverse effect can reduce the benefit of SPUD both upward and downward configuration with smaller gap between the two deflectors. Also, the reason for this is likely due to the fact that there is insignificant change in  $C_{p-ave}$  value as the deflector width increases. Noting that the optimum width,  $w_2$ , can only increase the  $C_{p-ave}$  value by about 5.5%, 1.3% and 1.7% compared to baseline SPUD at low, medium and high regimes of TSRs, respectively.

Furthermore, it is observed that the increment of deflector width has greater effect on the  $C_{p-ave}$  improvement at low regimes of TSRs compared to medium and high regimes of TSRs. The  $C_{mi}$  distributions shown in Figure 19 demonstrate that at low regime of TSRs, the change of width can improve the positive moment production and at same time reduce the negative moment production. However, at medium regime of TSRs, the change of width can enhance the positive moment production, but it also increases the negative moment production. Hence, the increment of width of SPUD cannot work effectively outside low regime of TSRs (Figure 20).

### Effects of inclination angle of upstream deflector

Following the investigation of the width variations of the deflector, simulation continues on investigating the effect of inclination angle ( $\theta_{SPUD}$ ) on the performance enhancement of VAWT (see Figure 21). The motivation behind this investigation comes from a convergence duct or nozzle configuration that can avoid the sudden change of flow, especially around the gap of deflectors, due to vertically arranged deflectors. By introducing an inclination angle, it is anticipated that the incoming flow speed can gradually increase before passing through the gap between deflectors compared to original SPUD configuration. The proposed angle variations can be seen in Table 6.

Table 7 gives the effect of  $\theta_{SPUD}$  on the  $C_{p-ave}$  value of VAWT at all regimes of TSRs. Interestingly, the introduction of three  $\theta_{SPUD}$  angles reduces the  $C_{p-ave}$  of VAWT at all regimes of TSRs, rather than increases it as initially anticipated. This is possibly due to the fact that adding inclination angle will reduce the effective width (i.e.,

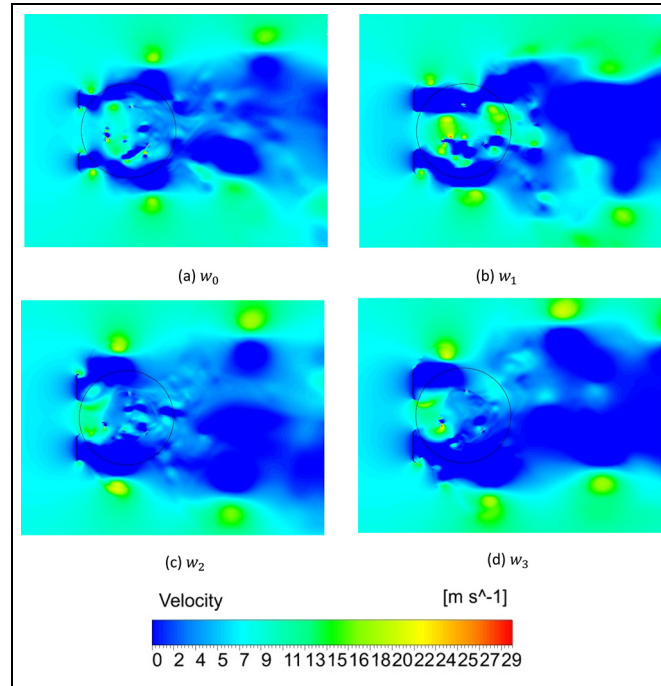


**Figure 19.** Comparison of velocity contours of VAWT with SPUD of four different widths (TSR = 2.64,  $\theta = 360^\circ$ ). The circles in dark solid lines represent the rotating core sub-domain.

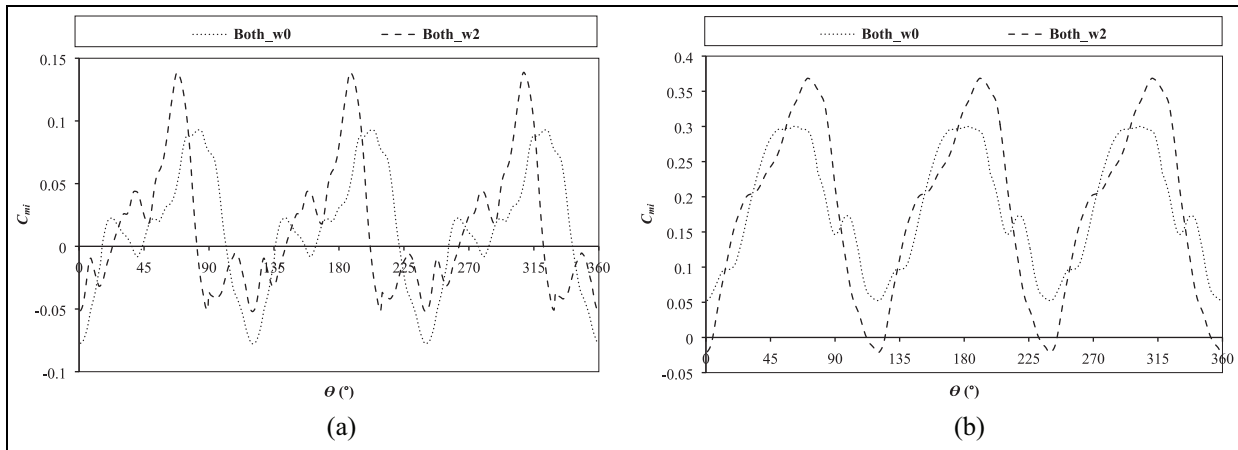


**Figure 20.** Comparison of  $C_{mi}$  distributions of VAWT with SPUD of four different widths (a) TSR = 1.44 and (b) TSR = 2.64.

**Table 6.** Variations of SPUD inclination angle.

| Case                             | Angle |
|----------------------------------|-------|
| $\theta_{SPUD0}$ (base geometry) | 0°    |
| $\theta_{SPUD1}$                 | 30°   |
| $\theta_{SPUD2}$                 | 45°   |
| $\theta_{SPUD3}$                 | 60°   |

the frontal area) of the deflector (see Figure 21), while the deflector is tilted. It has been shown in Section 4.2 that increment of the width of the deflector can enhance the  $C_{p-ave}$  value of VAWT, while reducing it will decrease the  $C_{p-ave}$  value of VAWT. To further confirm this, VAWT with SPUD using a reduced width of  $0.5w$  is studied. It is

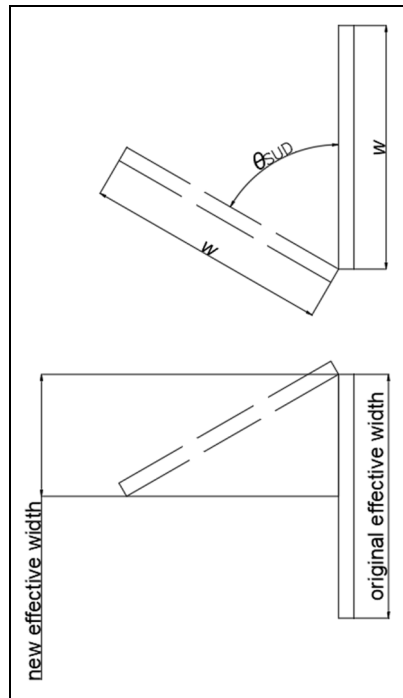


**Figure 21.** Inclination angle of SPUD (for both upward and downward configuration).

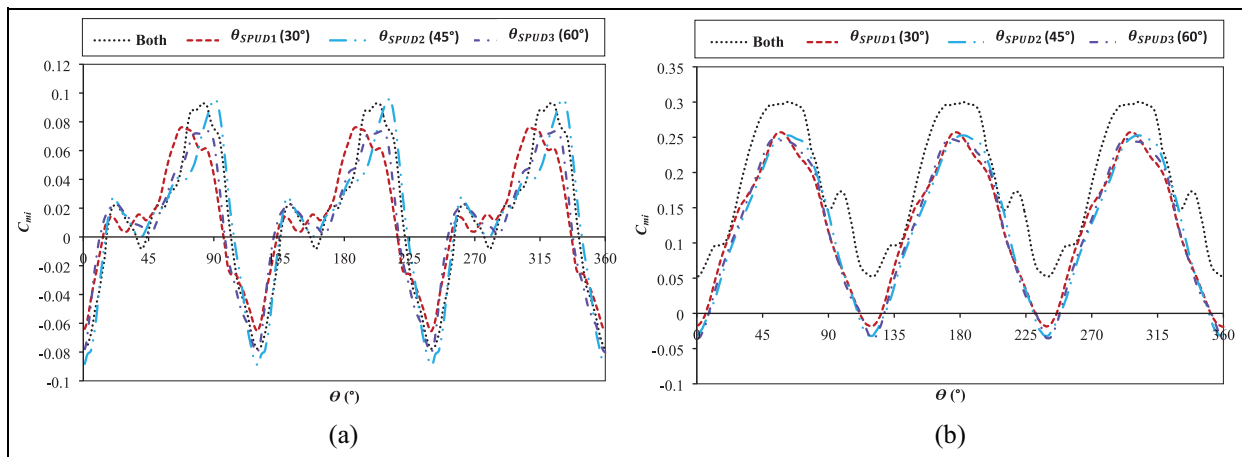


**Figure 22.** Comparison of the effect of inclination angle on the  $C_{mi}$  distribution of VAWT with SPUD at (a)  $TSR = 1.44$  and (b)  $TSR = 2.64$ .

noted that the  $C_{p-ave}$  value of VAWT with this thin SPUD decreases to 0.4126 compared to VAWT with base geometry of SPUD at  $TSR = 2.64$  ( $C_{p-ave} = 0.48459$ ), in agreement with those findings discussed above.

Further investigation shows that based on  $C_{mi}$  distributions at  $TSR = 2.64$  (see Figure 22), tilting the deflectors can reintroduce the negative moment production of VAWT and decrease its positive moment generation. Hence, the average moment production reduces, resulting in lower power generation. Introducing inclination angle of the deflectors also decreases the ability of deflectors to guide the wind towards the rotor area of the turbine. Figure 23 shows that the wind starts to ‘be shifted’ away from the blades of the turbine, as the deflectors are tilted. The wake region behind the deflector is also found to be shifted away from the blades of the turbine (see Figure 24). This wake region can be drifted further away from the blades as the inclination angle increases. This means that the blades of the turbine is no longer fully located behind the wake region of the upstream deflectors. Hence, the effect

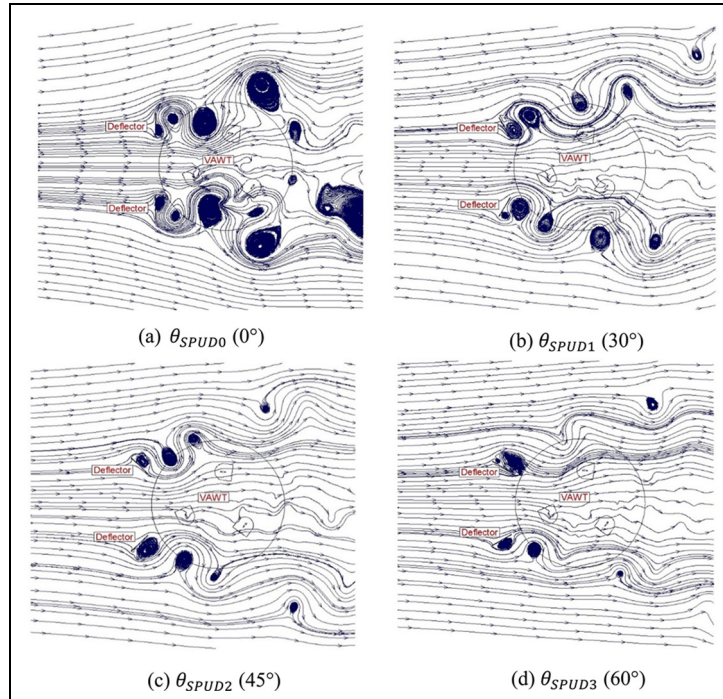


**Figure 23.** Comparison of streamlines of the flow around VAWT with SPUD at four different inclination angles (TSR = 2.64,  $\theta = 360^\circ$ ).

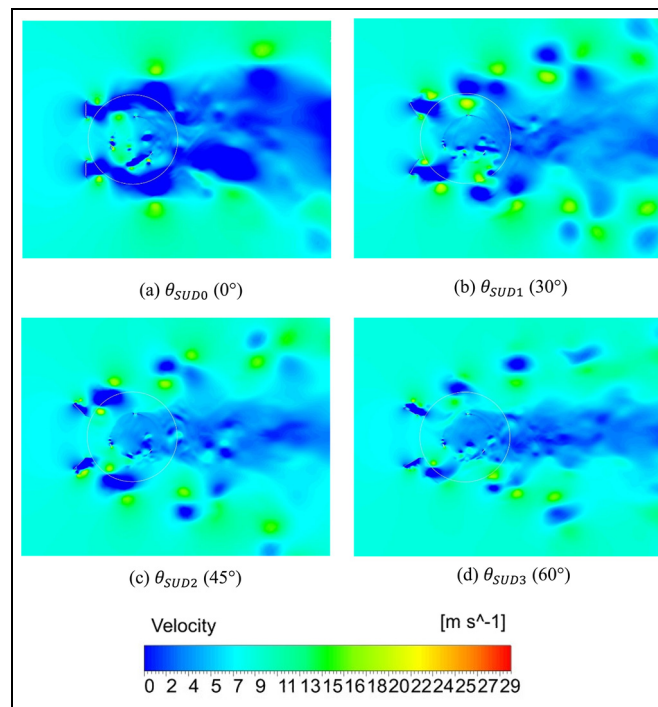


**Figure 24.** Comparison of velocity contours of VAWT with SPUD at four different inclination angles (TSR = 2.64,  $\theta = 360^\circ$ ). The circles in white solid lines represent the rotating core sub-domain.

of augmentation of SUPD to the wind speed reduces. As shown in Figure 24, the velocity of tilted deflectors is relatively lower compared to that of non-tilted deflectors around the blades of VAWT.

**Table 7.** Comparison of the effect of inclination angle on the  $C_{p-ave}$  of VAWT with SPUD.

| Case                             | $C_{p-ave}$ |            |           |
|----------------------------------|-------------|------------|-----------|
|                                  | TSR = 1.44  | TSR = 2.64 | TSR = 3.3 |
| Bare VAWT                        | 0.00850     | 0.31743    | 0.26166   |
| $\theta_{SPUD0}$ (base geometry) | 0.01927     | 0.48459    | 0.39907   |
| $\theta_{SPUD1}$                 | 0.01883     | 0.33771    | 0.29914   |
| $\theta_{SPUD2}$                 | 0.01745     | 0.32929    | 0.28589   |
| $\theta_{SPUD3}$                 | 0.01530     | 0.32699    | 0.28561   |

However, it is noted that the inclination angle can re-generate smooth  $C_{mi}$  distributions following the reduction of its fluctuation distributions caused by the existence of the deflectors. The streamlines illustrated in Figure 23 demonstrate that the tilted deflectors can decrease the vortex generation behind the deflectors, which can reduce the flow unsteadiness. However, this benefit cannot assist the tilted deflectors to further improve the performance of VAWT as it changes the main purposes of adding a deflector in upstream of VAWT (i.e., to enhance the local wind speed and to re-direct the wind towards the blades of turbine).

From Table 7, it can be seen that at medium (TSR = 2.64) and high (TSR = 3.3) regimes of TSRs, tilting the deflectors has worse effect on the decrement of  $C_{p-ave}$  value than at low regime of TSRs (TSR = 1.44). In fact, at medium and high regimes of TSRs, a deflector with inclination angle can reduce the  $C_{p-ave}$  almost down to the value of bare VAWT. Compared to base geometry of SPUD, SPUD with optimum inclination angle can decrease  $C_{p-ave}$  improvement significantly by about 87.8% and 72.7% at medium and high regimes of TSRs, respectively. Meanwhile at low regime of TSRs, the decrement of  $C_{p-ave}$  value is not that significant (only around 4.1% compared to the base geometry of SPUD). The  $C_{mi}$  distribution suggests that tilting the deflectors can increase the negative moment production at all regimes of TSRs (see Figure 22). However, while it can weaken the positive moment production at other regimes of TSRs, although tilting the deflectors can generally improve the positive moment production at low regimes of TSRs. Therefore, the decrease of average moment production, which leads to reduction of VAWT's power generation at low regimes of TSRs, is found not as strong as those at medium and high regimes of TSRs.

## Conclusion

The effect of straight plate upstream deflector on the performance enhancement of VAWT is studied and based on results obtained it can be concluded that the addition of deflector in upstream of VAWT can improve the VAWT performance at all regimes of TSRs. This is mainly because the existence of upstream deflector can enhance the incoming wind speed and help to direct the wind towards the rotor area of the turbine. However, the ability of SPUD to improve the performance of VAWT varies at each regime of TSRs. At low regime of TSRs, the  $C_{p-ave}$  enhancement can be up to about 126.7% while at medium and high regimes of TSRs. This enhancement is around 52.7% and 52.5%, respectively. This is caused by the fact that at low regime of TSRs, the enhancement of rotational speed has greater benefit to help the turbine in reducing negative moment production, which can lead to the improvement of self-starting ability and increase of power generation. However, higher rotational speed can also introduce the blockage effect and higher drag at medium and high regimes of TSRs, resulting in less improvement in power generation of VAWT.

Furthermore, it is very important to place the SPUD at the right location in upstream of VAWT. Based on  $C_{p-ave}$  value evaluation, it is found that placing deflectors at both upward and downward of the upstream of VAWT can generate the best improvement of power generation at all regimes of TSRs compared to the other three studied configurations (i.e., upward, middle and downward). The gap between the two deflectors in both upward and downward configuration introduces a converged duct/nozzle flow effect, which can further enhance the incoming wind speed. Adding deflectors at both upward and downward locations can also direct the wind towards the turbines of VAWT, resulting in higher mass flow rate of wind directed to the rotor area of the turbine. Moreover, compared to the other three SPUD configurations (i.e., upward, middle and downward), the blades of VAWT in both upward and downward configuration can largely mitigate the upstream deflector wake by not directly impinging onto the downstream blades when they are rotating. Thus, this configuration is better to improve the  $C_{p-ave}$  value of VAWT.

After identifying the best configuration of SPUD, further parametric studies have been performed focussing on the width and inclination angle of SPUD. It is found that the increment of the deflector width has slightly positive effect on the increment of  $C_{p-ave}$  value of VAWT as long as the positive influence of narrower gap between the two deflectors can withstand the impact of larger wake region caused by a wider deflector. SPUD with optimum width (150% of  $w_0$ ) can further enhance the  $C_{p-ave}$  improvement by 5.5%, 1.2% and 1.7% at low, medium and high regimes of TSRs, respectively. On the other hand, adding inclination angle to the SPUD produces worse  $C_{p-ave}$  improvement than SPUD without inclination angle. Surprisingly, while tilting deflectors indeed can reduce the vortex generation behind the straight (vertical) deflector to reduce flow unsteadiness, the reduction in effective width can decrease the  $C_{p-ave}$  value of VAWT. The tilting deflectors can also re-direct the incoming wind away from the blades of the turbine, causing the reduction of the ability of the deflectors to direct the wind to the blades of VAWT. Therefore, both upward and downward configuration with original (vertical arranged) geometry is more acceptable as a SPUD design to improve the performance of VAWT. If the drawback of the addition of the weight caused by the width increment can be overcome (e.g., using lighter materials such as composite), the width of the deflector can be increased to 150% of  $w_0$  to gain further performance improvement.

It is worth to note that this study has not investigated the effects of the thickness of SUPD and its position in the  $x$ -direction. This study adopted the findings from a previous study (Kim and Gharib, 2013) on the thickness of SUPD and its the  $x$ -direction position, because of same regime of Reynold number in these two studies. Hence, future study could be carry out on to understand the effects of these two parameters on the performance improvement of VAWT. Additionally, experimental study would be valuable to validate the findings from numerical studies. However they are outside the scope of this study.


### Declaration of conflicting interests

The author(s) declared no potential conflicts of interest with respect to the research, authorship, and/or publication of this article.

### Funding

The author(s) disclosed receipt of the following financial support for the research, authorship, and/or publication of this article: The first author would like to acknowledge the Ministry of Education, Culture, Research and Technology of Indonesia and Indonesian Endowment Fund for Education (LPDP) of the Ministry of Finance of Indonesia for the financial support through BUDI LPDP scholarship (Reference Letter Number: S-1166/LPDP.3/2017).

### ORCID iD

Taurista P. Syawitri  <https://orcid.org/0000-0002-3693-1881>

### References

- Acarer S (2020) Peak lift-to-drag ratio enhancement of the DU12W262 airfoil by passive flow control and its impact on horizontal and vertical axis wind turbines. *Energy* 201, 117659. <https://doi.org/10.1016/j.energy.2020.117659>.
- ANSYS, Inc. (2020) ANSYS Fluent User's Guide, Release 19.1.
- Bakırcı M and Yılmaz S (2018) Theoretical and computational investigations of the optimal tip-speed ratio of horizontal-axis wind turbines. *Engineering Science and Technology, an International Journal* 21(6): 1128–1142. <https://doi.org/10.1016/j.jestech.2018.05.006>.
- Balduzzi F, Bianchini A, Maleci R, et al. (2016) Critical issues in the CFD simulation of Darrieus wind turbines. *Renewable Energy* 85: 419–435. <https://doi.org/10.1016/j.renene.2015.06.048>.
- Bianchini A, Balduzzi F, Bachant P, et al. (2017) Effectiveness of two-dimensional CFD simulations for Darrieus VAWTs: A combined numerical and experimental assessment. *Energy Conversion and Management* 136: 318–328. <https://doi.org/10.1016/j.enconman.2017.01.026>.
- Bianchini A, Balduzzi F, Rosa DD, et al. (2019) On the use of gurney flaps for the aerodynamic performance augmentation of Darrieus wind turbines. *Energy Conversion and Management* 184: 402–415. <https://doi.org/10.1016/j.enconman.2019.01.068>.
- Castelli MR, Englaro A and Benini E (2011) The Darrieus wind turbine: Proposal for a new performance prediction model based on CFD. *Energy* 36: 4919–4934. <https://doi.org/10.1016/j.energy.2011.05.036>.
- Chen J, Yang H, Yang M, et al. (2015) The effect of the opening ratio and location on the performance of a novel vertical axis Darrieus turbine. *Energy* 89: 819–834. <https://doi.org/10.1016/j.energy.2015.05.136>.
- Chong WT, Fazlizan A, Poh SC, et al. (2013) The design, simulation and testing of an urban vertical axis wind turbine with the omni-direction-guide-vane. *Applied Energy* 112: 601–609. <https://doi.org/10.1016/j.apenergy.2012.12.064>.

- Choudhry A, Arjomandi M and Kelso R (2016) Methods to control dynamic stall for wind turbine applications. *Renewable Energy* 86: 26–37. <https://doi.org/10.1016/j.renene.2015.07.097>.
- Dixon K (2008) *The near wake structure of a vertical axis wind turbine*. Master Thesis ed., Delft University of Technology, Delft.
- Frank T and Menter F (2017) Validation of URANS SST and SBES in ANSYS CFD for the turbulent mixing of two parallel planar water jets impinging on a stationary pool validation of URANS SST and SBES in ANSYS CFD for the turbulent mixing of two parallel planar water jets impinging on a stationary pool. *Proceedings of the ASME 2017 Verification and Validation Symposium*, 3–5 May, 2017, ASME, Las Vegas.
- Ghazalla RA, Mohamed MH and Hafiz AA (2019) Synergistic analysis of a Darrieus wind turbine using computational fluid dynamics. *Energy*, 189: 116214. <https://doi.org/10.1016/j.energy.2019.116214>.
- Jin X, Wang Y, Ju W, et al. (2018) Investigation into parameter influence of upstream deflector on vertical axis wind turbines output power via three-dimensional CFD simulation. *Renewable Energy*, 115: 41–53. <https://doi.org/10.1016/j.renene.2017.08.012>.
- Kim D and Gharib M (2013) Efficiency improvement of straight-bladed vertical-axis wind turbines with an upstream deflector. *Journal of Wind Engineering and Industrial Aerodynamics* 115: 48–52. <https://doi.org/10.1016/j.jweia.2013.01.009>.
- Kim D and Gharib M (2014) Unsteady loading of a vertical-axis turbine in the interaction with an upstream deflector. *Experiments in Fluids* 55: 1658. <https://doi.org/10.1007/s00348-013-1658-4>.
- Lanzafame R, Mauro S, Messina M, et al. (2020) Development and validation of CFD 2D models for the simulation of micro H-Darrieus turbines subjected to high boundary layer instabilities. *Energies* 13: 5564. <https://doi.org/10.3390/en13215564>.
- Letizia S and Zanforlin S (2016) Hybrid CFD-source terms modelling of a diffuser-augmented vertical axis wind turbine. *Energy Procedia* 101: 1280–1287. <https://doi.org/10.1016/j.egypro.2016.11.144>.
- Malael I, Dumitrescu H and Cardos V (2014) Numerical simulation of vertical axis wind turbine at low speed ratios. *Global Journal of Researches in Engineering: I Numerical Methods* 14(1): 9–20.
- Menter F (2018) Stress-blended eddy simulation (SBES)-A new paradigm in hybrid RANS-LES modeling. *Notes on Numerical Fluid Mechanics and Multidisciplinary Design* 137: 27–37. [https://doi.org/10.1007/978-3-319-70031-1\\_3](https://doi.org/10.1007/978-3-319-70031-1_3).
- Mohamed OS, Ibrahim AA, Etman AK, et al. (2020) Numerical investigation of Darrieus wind turbine with slotted airfoil blades. *Energy Conversion and Management X* 5: 100026. <https://doi.org/10.1016/j.ecmx.2019.100026>.
- Nobile R, Vahdati M, Barlow JF, et al. (2014) Unsteady flow simulation of a vertical axis augmented wind turbine: A two-dimensional study. *Journal of Wind Engineering and Industrial Aerodynamics* 125: 168–179. <https://doi.org/10.1016/j.jweia.2013.12.005>.
- Ragheb M and Ragheb AM (2011) Wind turbine theory-the betz equation and optimum rotor tip speed ratio. In: Carriveau R (ed) *Fundamental and Advanced Topics in Wind Power*. London, UK: InTech, Rijeka, Croatia, pp.19–38. <https://doi.org/10.5772/21398>.
- Rezaeiha A, Kalkman I and Blocken B (2017) CFD simulation of a vertical axis wind turbine operating at a moderate tip speed ratio: Guidelines for minimum domain size and azimuthal increment. *Renewable Energy* 107: 373–385. <https://doi.org/10.1016/j.renene.2017.02.006>.
- Rezaeiha A, Montazeri H and Blocken B (2018a) Characterization of aerodynamic performance of vertical axis wind turbines: Impact of operational parameters. *Energy Conversion and Management* 169: 45–77. <https://doi.org/10.1016/j.enconman.2018.05.042>.
- Rezaeiha A, Montazeri H and Blocken B (2018b) Towards accurate CFD simulations of vertical axis wind turbines at different tip speed ratios and solidities: Guidelines for azimuthal increment, domain size and convergence. *Energy Conversion and Management* 156: 301–316. <https://doi.org/10.1016/j.enconman.2017.11.026>.
- Rezaeiha A, Montazeri H and Blocken B (2019) On the accuracy of turbulence models for CFD simulations of vertical axis wind turbines. *Energy* 180: 838–857. <https://doi.org/10.1016/j.energy.2019.05.053>.
- Sobhani E, Ghaffari M and Maghrebi MJ (2017) Numerical investigation of dimple effects on darrieus vertical axis wind turbine. *Energy* 133: 231–241.
- Stout C, Islam S, White A, et al. (2017) Efficiency improvement of vertical axis wind turbines with an upstream deflector. *Energy Procedia* 118: 141–148. <https://doi.org/10.1016/j.egypro.2017.07.032>.
- Syawitri TP, Yao YF, Chandra B, et al. (2021) Comparison study of URANS and hybrid RANS-LES models on predicting vertical axis wind turbine performance at low, medium and high tip speed ratio ranges. *Renewable Energy* 168: 247–269. <https://doi.org/10.1016/j.renene.2020.12.045>.
- Syawitri TP, Yao YF, Yao J, et al. (2020) Assessment of stress-blended eddy simulation model for accurate performance prediction of vertical axis wind turbine. *International Journal of Numerical Methods for Heat & Fluid Flow* 31(2): 655–673. <https://doi.org/10.1108/HFF-09-2019-0689>.
- Takao M, Kuma MH, Maeda T, et al. (2009) A straight-bladed vertical axis wind turbine with a directed guide vane row-effect of guide vane geometry on the performance. *Journal of Thermal Science* 18(1): 54–57. <https://doi.org/10.1007/s11630-009-0054-0>.
- Wang Y, Lia G, Shen S, et al. (2018) Investigation on aerodynamic performance of horizontal axis wind turbine by setting micro-cylinder in front of the blade leading edge. *Energy* 143: 1107–1124. <https://doi.org/10.1016/j.energy.2017.10.094>.

- Watanabe K, Takahashi S and Ohya Y (2016) Application of a diffuser structure to vertical-axis wind turbines. *Energies* 9(6): 406. <https://doi.org/10.3390/en9060406>.
- Wong KH, Chong WT, Sukiman NL, et al. (2017) Performance enhancements on vertical axis wind turbines using flow augmentation systems: A review. *Renewable and Sustainable Energy Reviews* 73: 904–921. <https://doi.org/10.1016/j.rser.2017.01.160>.
- Wong KH, Chong WT, Poh SC, et al. (2018a) 3D CFD simulation and parametric study of a flat plate deflector for vertical axis wind turbine. *Renewable Energy* 129: 32–55. <https://doi.org/10.1016/j.renene.2018.05.085>.
- Wong KH, Chong WT, Sukiman NL, et al. (2018b) Experimental and simulation investigation into the effects of a flat plate deflector on vertical axis wind turbine. *Energy Conversion and Management* 160: 109–125. <https://doi.org/10.1016/j.enconman.2018.01.029>.
- Wong KH, Chong WT, Yap HT, et al. (2014) The design and flow simulation of a power-augmented shroud for urban wind turbine system. *Energy Procedia* 61: 1275–1278. <https://doi.org/10.1016/j.egypro.2014.11.1080>.
- Yan Y, Avital E and Williams J (2019a) CFD analysis for the performance of gurney flap on aerofoil and vertical axis turbine. *International Journal of Mechanical Engineering and Robotics Research* 8(3): 385–392. <https://doi.org/10.18178/ijmerr.8.3.385-392>.
- Yan Y, Avital E, Williams J, et al. (2019b) CFD analysis for the performance of micro-vortex generator on aerofoil and vertical axis turbine. *Journal of Renewable and Sustainable Energy* 11(4): 043302. <https://doi.org/10.1063/1.5110422>.
- Yan Y, Avital E, Williams J, et al. (2020) Performance improvements for a vertical axis wind turbine by means of gurney flap. *Journal of Fluids Engineering* 142(2): 15. <https://doi.org/10.1115/1.4044995>.
- Zhu H, Hao W, Li C, et al. (2018) Simulation on flow control strategy of synthetic jet in a vertical axis wind turbine. *Aerospace Science and Technology* 77: 439–448. <https://doi.org/10.1016/j.ast.2018.03.012>.